

Electronic Supplementary Information

Phosphorus-Mo₂C@Carbon Nanowires toward Efficient Electrochemical Hydrogen Evolution: Composition, Structural and Electronic Regulation

Zhangping Shi,^a Kaiqi Nie,^d Zheng-Jiang Shao,^c Boxu Gao,^a Huanlei Lin,^b Hongbin Zhang,^a Bolun Liu,^a Yangxia Wang,^a Yahong Zhang,^a Xuhui Sun,^{*d} Xiao-Ming Cao,^{*c} P. Hu,^c Qingsheng Gao^{*b} and Yi Tang^{*a}

^a Shanghai Key Laboratory of Molecular Catalysis and Innovative Materials, Laboratory of Advanced Materials and Collaborative Innovation Center of Chemistry for Energy Materials, Department of Chemistry, Fudan University, Shanghai 200433, P. R. China. E-mail: yitang@fudan.edu.cn.

^b Department of Chemistry, Jinan University, Guangzhou 510632, P. R. China. E-mail: tqsgao@jnu.edu.cn.

^c Key Laboratory for Advanced Materials, Center for Computational Chemistry and Research Institute of Industrial Catalysis, School of Chemistry and Molecular Engineering, East China University of Science & Technology, Shanghai 200237, P. R. China. E-mail: xmcao@ecust.edu.cn.

^d Institute of Functional Nano & Soft Materials (FUNSOM) & Jiangsu Key Laboratory for Carbon-Based Functional Materials & Devices, Soochow University, Suzhou 215123, P. R. China. E-mail: xhsun@suda.edu.cn.

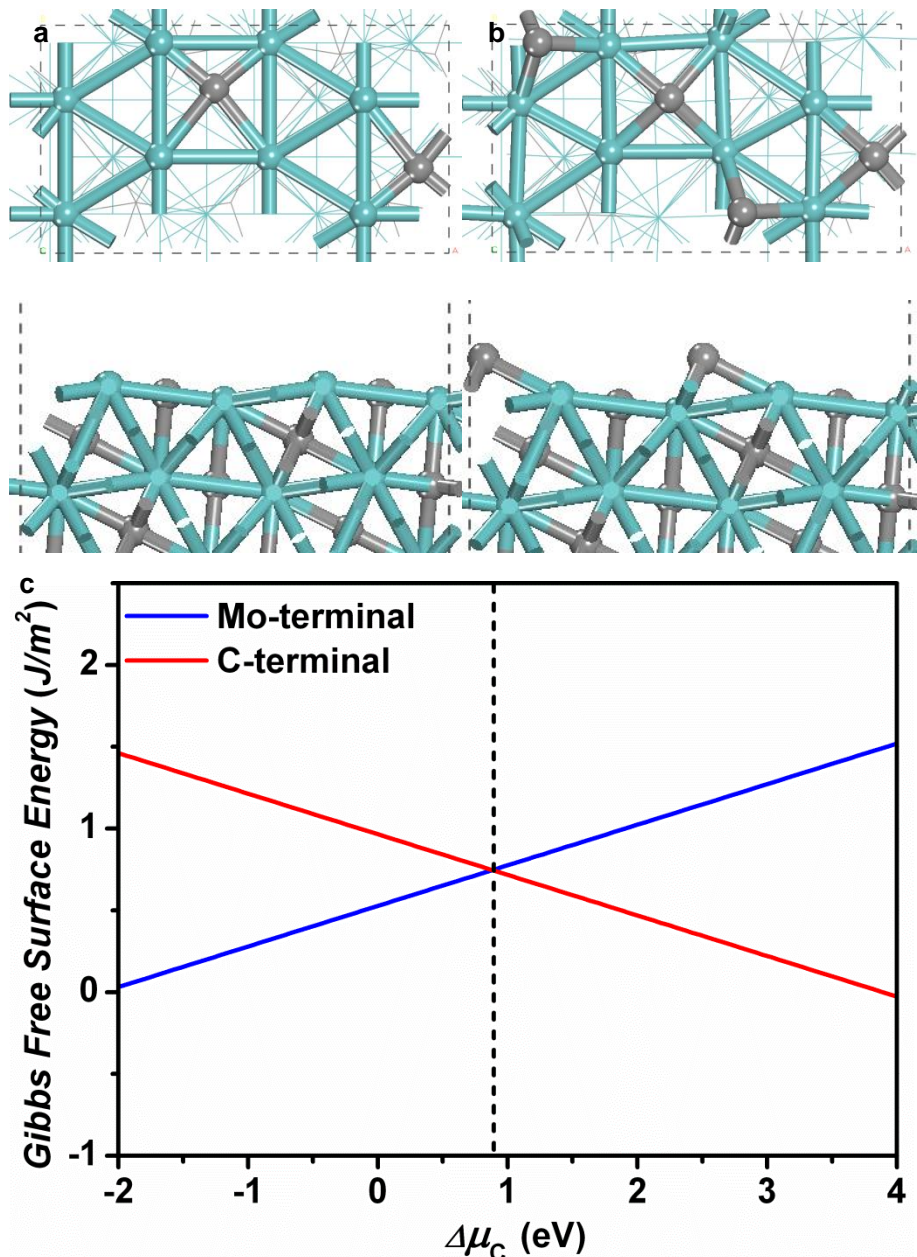


Fig. S1. Top (the first row) and side (the second row) views of (a) Mo-terminal of $\beta\text{-Mo}_2\text{C}$ (102) and (b) C-terminal of $\beta\text{-Mo}_2\text{C}$ (102); (c) Gibbs free surface energies of Mo-terminal of $\beta\text{-Mo}_2\text{C}$ (102) and C-terminal of $\beta\text{-Mo}_2\text{C}$ (102) as a function of $\Delta\mu_C$, using the chemical potential of C in gaseous CH_4 at 0 K as the zero reference. At HER reaction condition ($T = 298.15$ K), $\Delta\mu_C = -0.23$ eV, Mo-terminal is energetically more favorable than C-terminal.

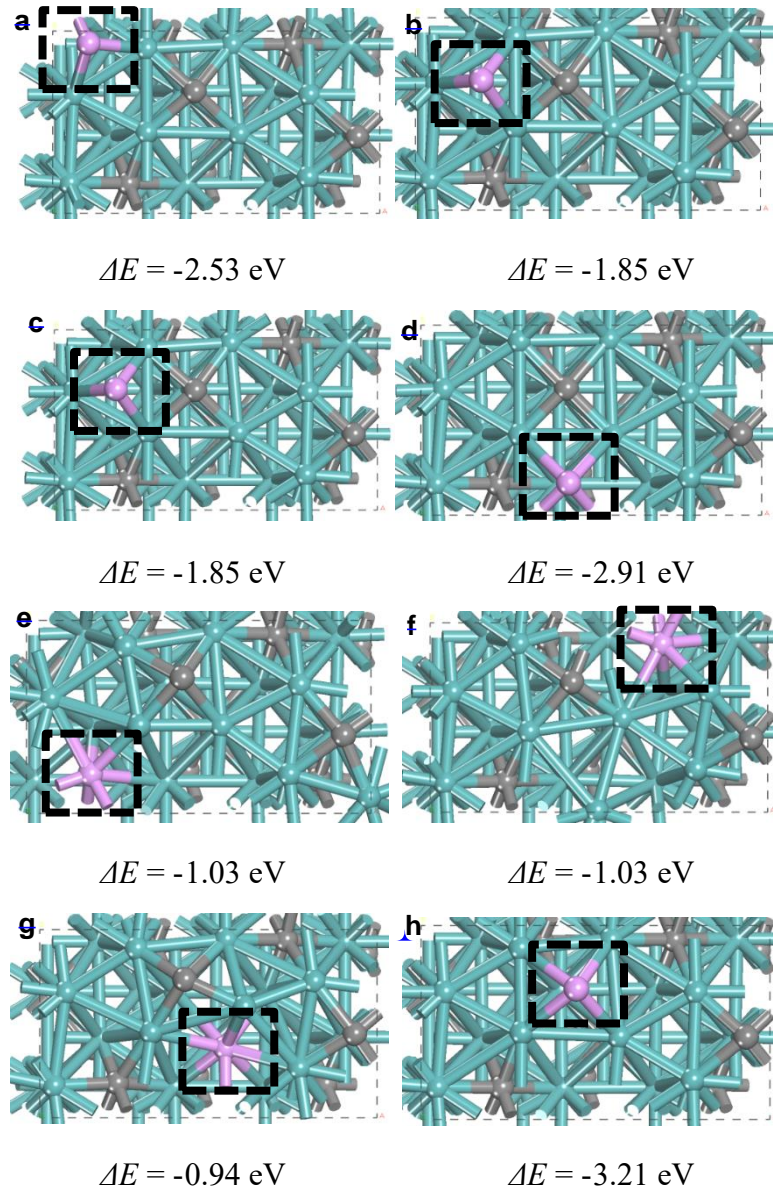


Fig. S2. Top views of possible 1P doped β -Mo₂C (102) after geometry optimization (The Mo, C, and P atoms are respectively displayed in cyan, grey, and pink. The black dashed box marks the original site of P at subsurface before geometry optimization) and the reaction energies with reference to the chemical potential of P at gaseous PH₃ and the chemical potential of C at CH₄: (a) P initially locates at free subsurface tetrahedral interstice site. After optimization, P migrates to the surface hcp site; (b) P initially locates at free subsurface octahedral interstice site. After optimization, P migrates to the surface fcc site; (c) P initially locates at free subsurface tetrahedral interstice site. After optimization, P migrates to the surface fcc site; (d) P initially locates at free b5 site (4-fold hollow). After optimization, P migrates to the surface 4-fold hollow site; (e) P replaces subsurface 6-fold C; (f) P replaces another subsurface 6-fold C (g) P replaces subsurface 5-fold C; (h) P replaces surface C at b5 site. Since the substitution of C at b5 site with P is energetically most stable followed by occupying the free b5 site, the doped P atoms energetically prefer to take place of the surface C atoms at the b5 sites firstly and with the increasing P content, they will occupy the free.

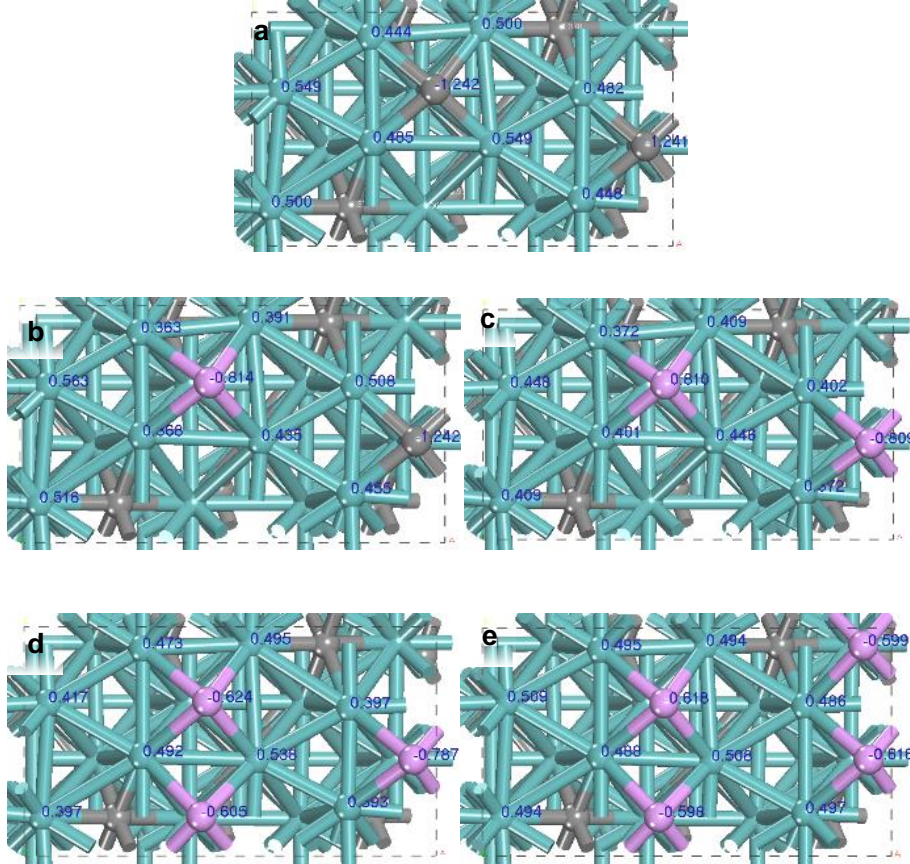


Fig. S3. The top view of (a) pristine Mo_2C (102), (b) 1P- Mo_2C (102), (c) 2P- Mo_2C (102), (d) 3P- Mo_2C (102), and (e) 4P- Mo_2C (102) and the Bader charges of the surface exposed atoms are marked in blue. The Mo, C, and P atoms are respectively displayed in cyan, grey, and pink. For P doped β - Mo_2C (102) surface, the P atoms are possible to occupy the vacant interstice sites or to replace the C atoms at Mo_2C . The first doped P energetically prefers to take place of one surface C atom in the 4-fold hollow site. Moreover, due to the greater atom radii of P atom compared with C atom, after substituting C atom, the doped P atom tends to rise from the 4-fold hollow site over the surface. This optimized geometry structure is analogical to the adsorption of P on the Mo-terminal of β - Mo_2C (102) surface with a surface C vacancy. With the increase of P-doping concentration, the second doped P preferentially replaces another surface C atom at 4-fold hollow site while both the third and the fourth doped P atoms energetically tend to occupy the free 4-fold hollow sites.

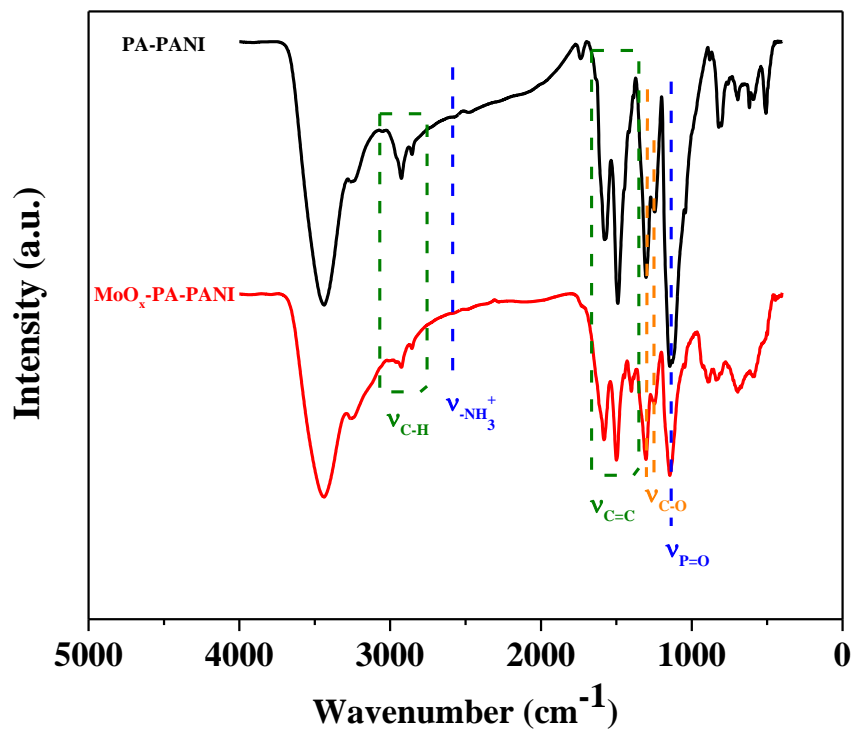


Fig. S4. FT-IR spectra of PA-PANI and MoO_x-PA-PANI hybrids of P-Mo₂C@C-2.9.

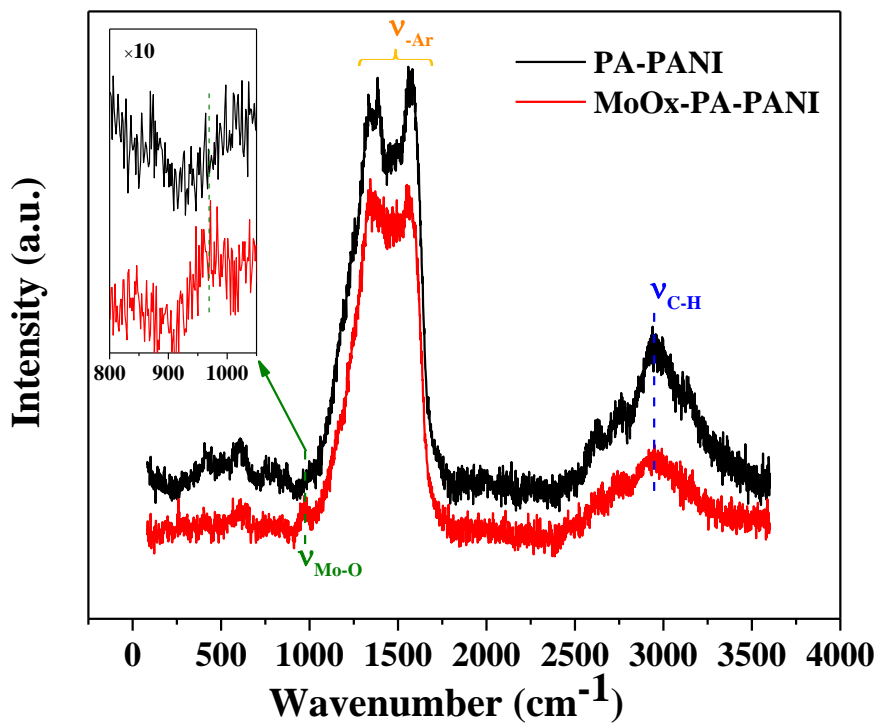


Fig. S5. Raman spectra of PA-PANI and MoO_x-PA-PANI hybrids of P-Mo₂C@C-2.9.

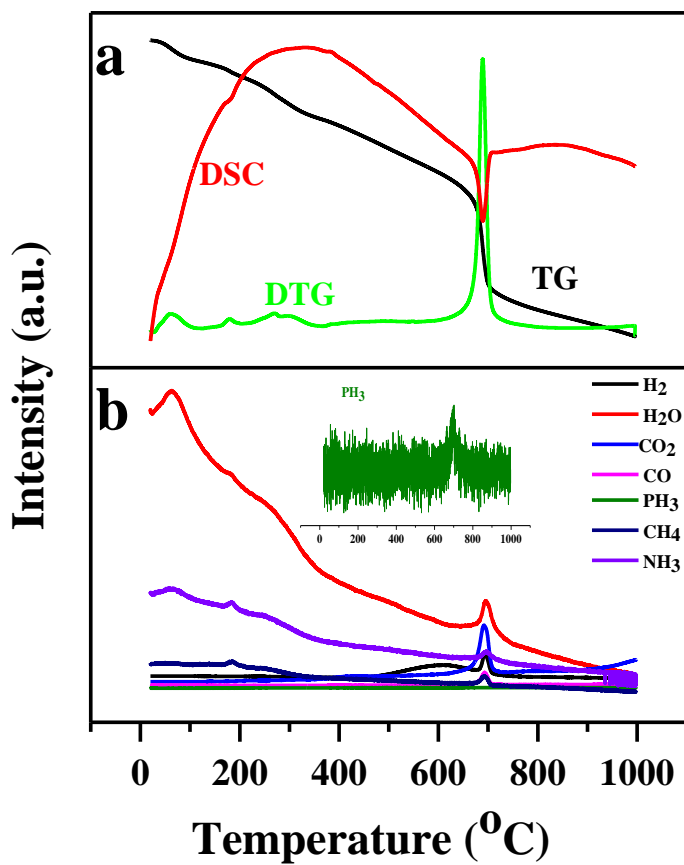


Fig. S6. Thermal analysis (a) of $\text{MoO}_x\text{-PA-PANI}$ precursor of P-Mo₂C@C-2.9 in N_2 , and the corresponding MS signals (b) of the mainly decomposed gases.

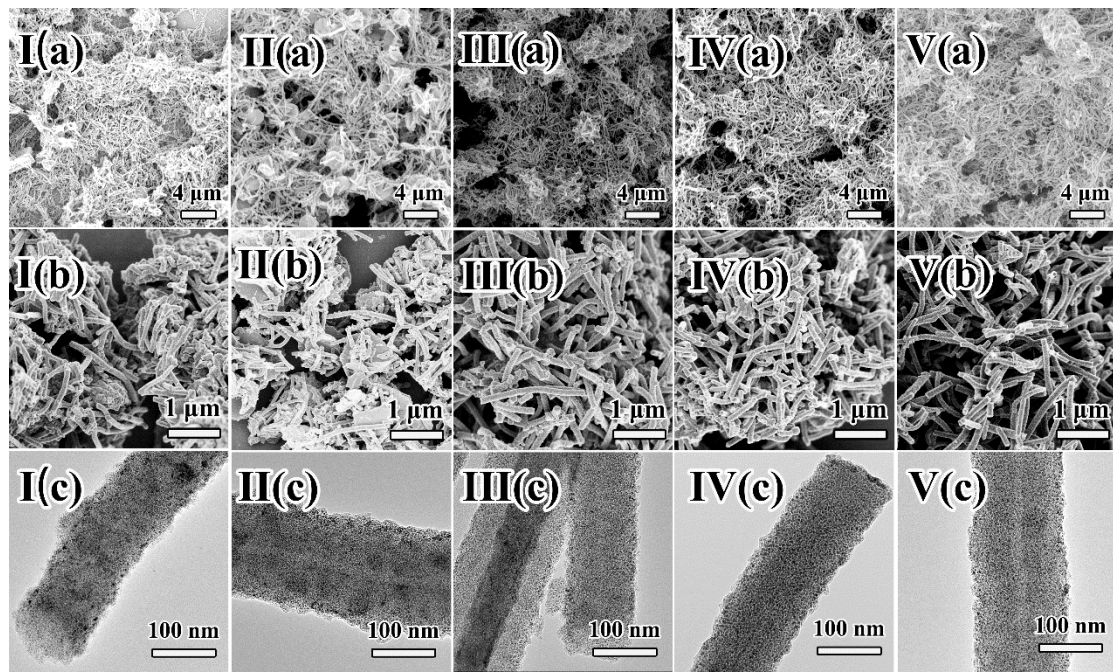
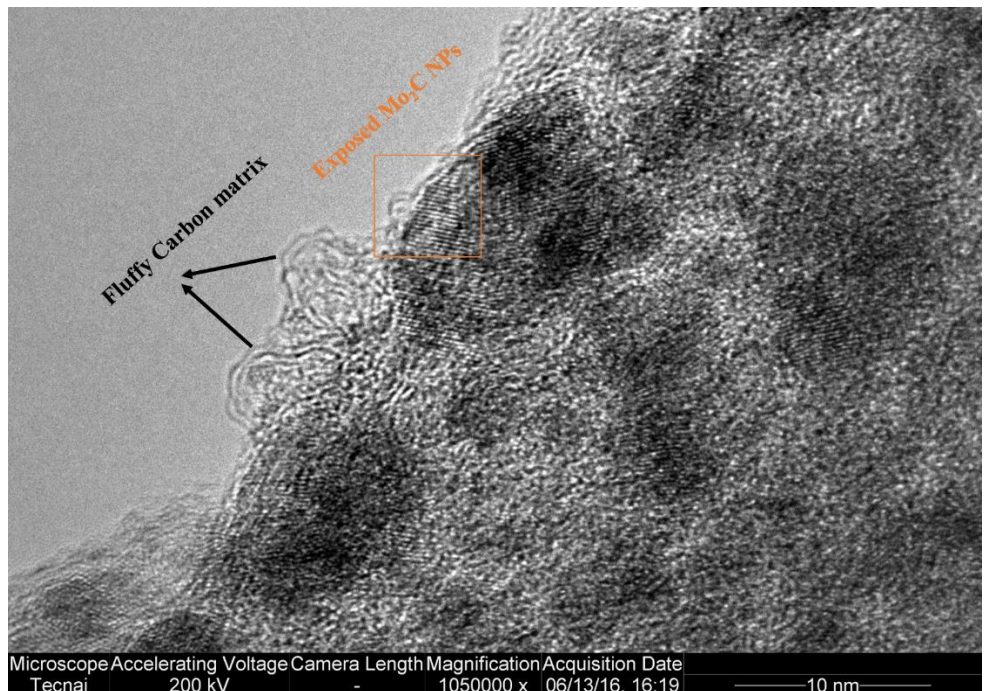


Fig. S7. SEM images of PA-PANI hybrids (I(a)~V(a)), SEM and TEM images of the corresponding electrocatalysts of Mo₂C@C (I(b, c)), P-Mo₂C@C-0.8 (II(b, c)), P-Mo₂C@C-1.9 (III(b, c)), P-Mo₂C@C-2.9 (IV(b, c)), and P-Mo₂C@C-3.4 (V(b, c)).



Microscope Accelerating Voltage Camera Length Magnification Acquisition Date
Tecnai 200 kV - 1050000 x 06/13/16, 16:19 10 nm

Fig. S8. HRTEM of P-Mo₂C@C-2.9 sample.

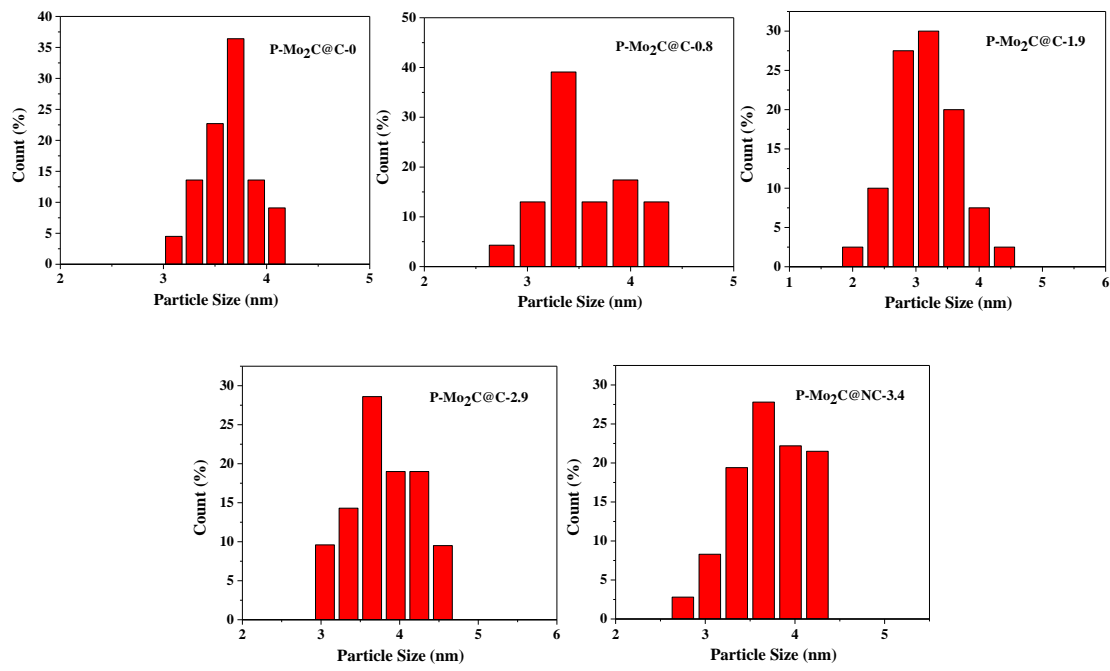


Fig. S9. Particle size distributions of β -Mo₂C NPs in P-Mo₂C@C NWs, respectively.

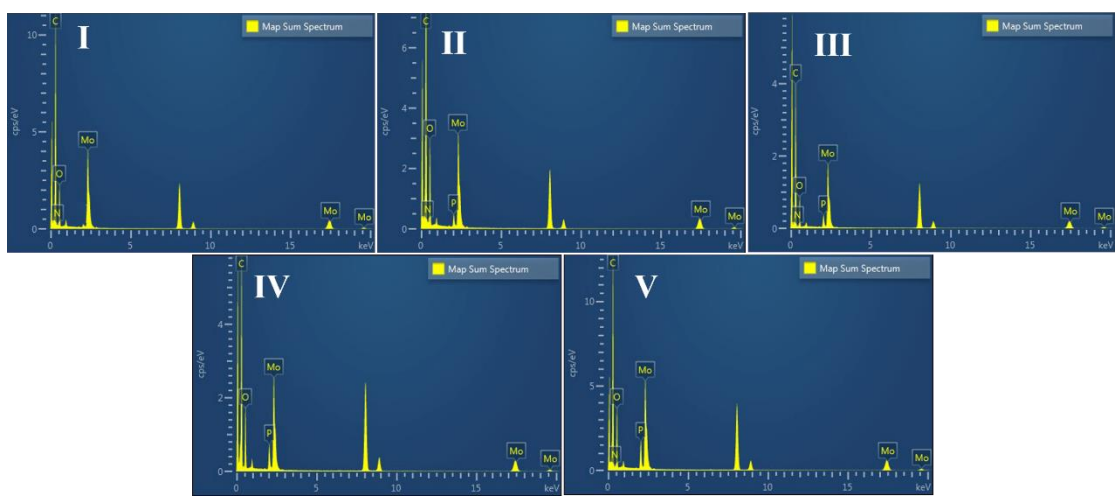


Fig. S10. EDS spectra of (I) $\text{Mo}_2\text{C}@\text{C}$, (II) $\text{P}-\text{Mo}_2\text{C}@\text{C}-0.8$, (III) $\text{P}-\text{Mo}_2\text{C}@\text{C}-1.9$, (IV) $\text{P}-\text{Mo}_2\text{C}@\text{C}-2.9$, and (V) $\text{P}-\text{Mo}_2\text{C}@\text{C}-3.4$.

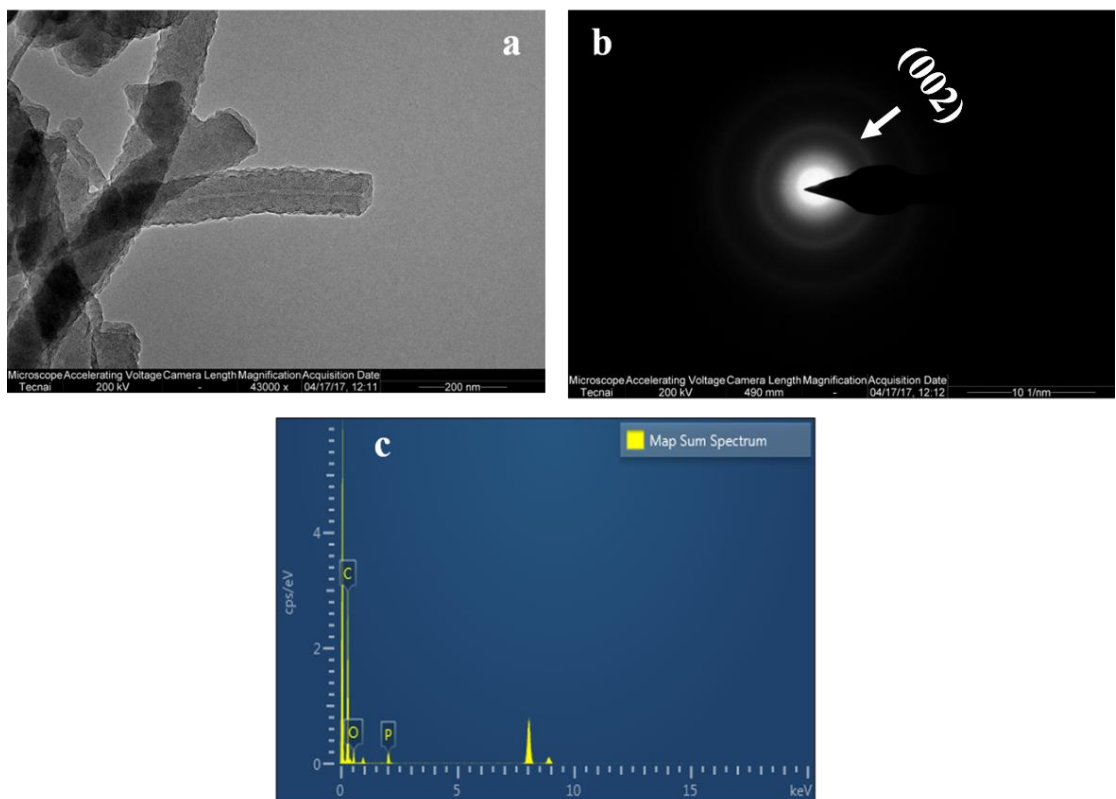


Fig. S11. (a) TEM, (b) SAED and (c) element analysis of (I) carbon matrix obtained via pyrolysis of PA-PANI hybrids with the same PA/aniline ratio as P-Mo₂C@C-2.9.

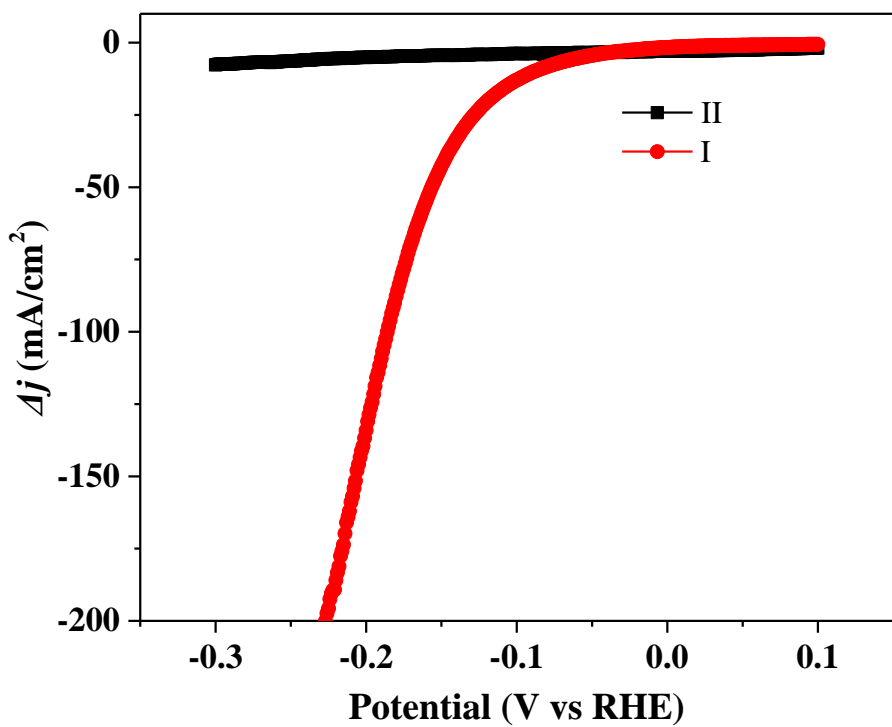


Fig. S12. (a) Polarization curves of (I) P-Mo₂C@C-2.9, (II) carbon matrix obtained via pyrolysis of PA-PANI hybrids with the same PA/aniline ratio as P-Mo₂C@C-2.9 in 0.5 M H₂SO₄ with the mass loading of 1.30 mg/cm².

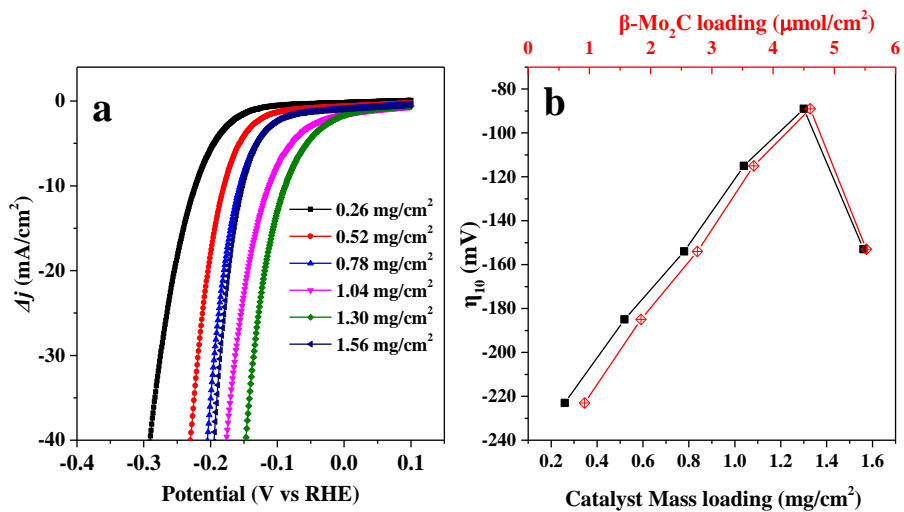


Fig. S13. (a) Polarization curves of P-Mo₂C@C-2.9 under different mass loadings, and (b) the relationships between mass loadings with η_{10} in 0.5 M H₂SO₄.

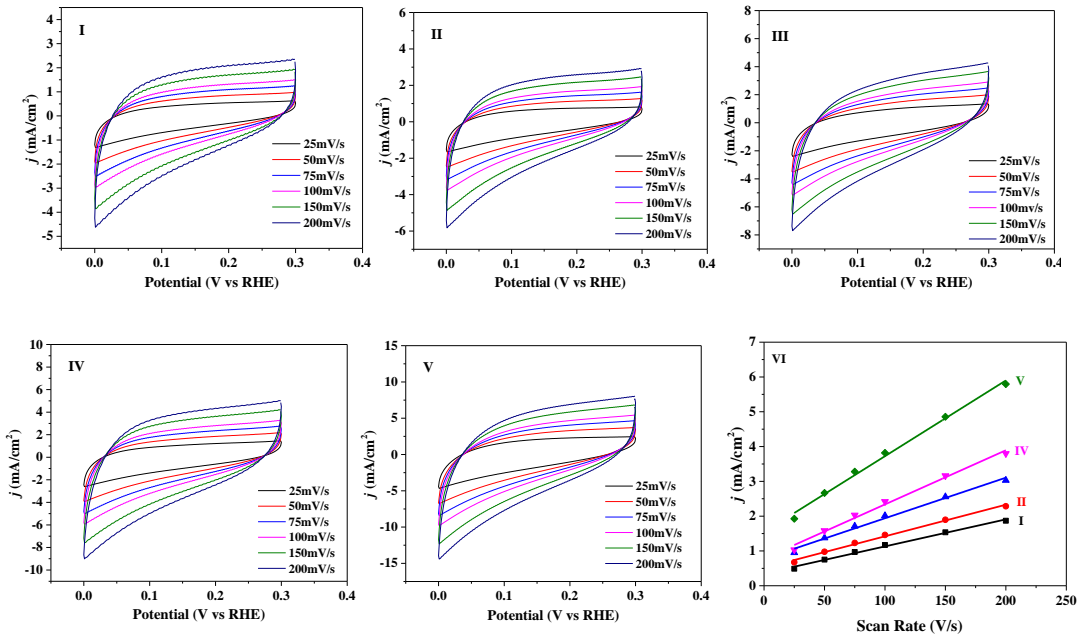


Fig. S14. Cyclic voltammograms of (I) Mo₂C@C, (II) P-Mo₂C@C-0.8, (III) P-Mo₂C@C-1.9, (IV) P-Mo₂C@C-2.9, and (V) P-Mo₂C@C-3.4 with different scan rates from 25 to 200 mV/s in the potential range of 0-0.3 V in 0.5 M H₂SO₄, and (VI) Estimation of C_{dl} by plotting the current density variation ($\Delta j = (j_a - j_c)/2$, at 150 mV vs. RHE) against scan rate to fit a linear regression.

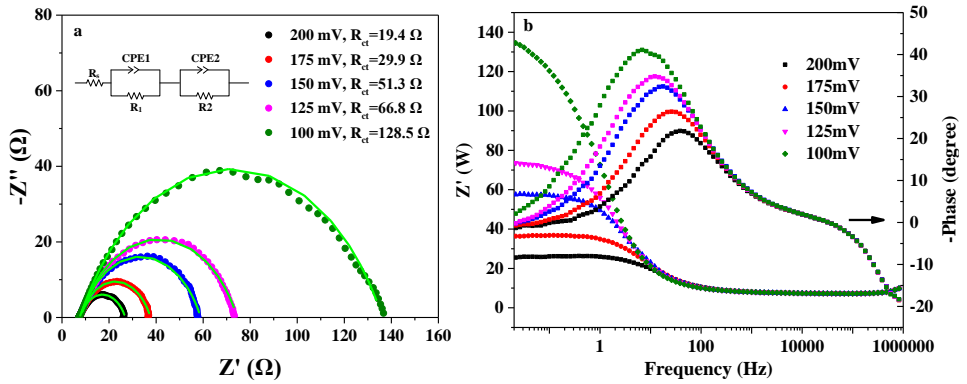


Fig. S15. (a) Electrochemical impedance spectroscopy of P-Mo₂C@C-2.9 under different overpotential, (b) Nyquist and Bode plots showing EIS responses of P-Mo₂C@C-2.9 at various HER overpotentials in 0.5 M H₂SO₄. ESI are fitted to the simplified equivalent circuit shown in the inset (a), and the fitting results are plotted as solid traces. Inset is the Equivalent circuit model for electrochemical impedance tests. R_s, R₁ and R₂ represent the electrolyte, electrode porosity and charge transfer resistance, respectively. CPE is the constant phase angle element, which represents the double layer capacitance of solid electrode in the real-world situation.

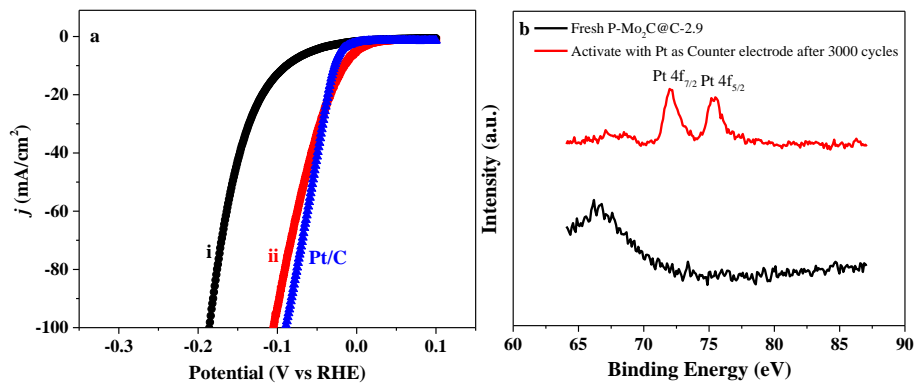


Fig. S16. (a) Polarization curves of (i) P-Mo₂C@C-2.9 with graphite rod as counter electrode, (ii) P-Mo₂C@C-2.9 after 3000 cycles with Pt as counter electrodes, and Pt/C; (b) the corresponding Pt-XPS spectra of fresh P-Mo₂C@C-2.9 and that after 3000 cycles with Pt as counter electrodes.

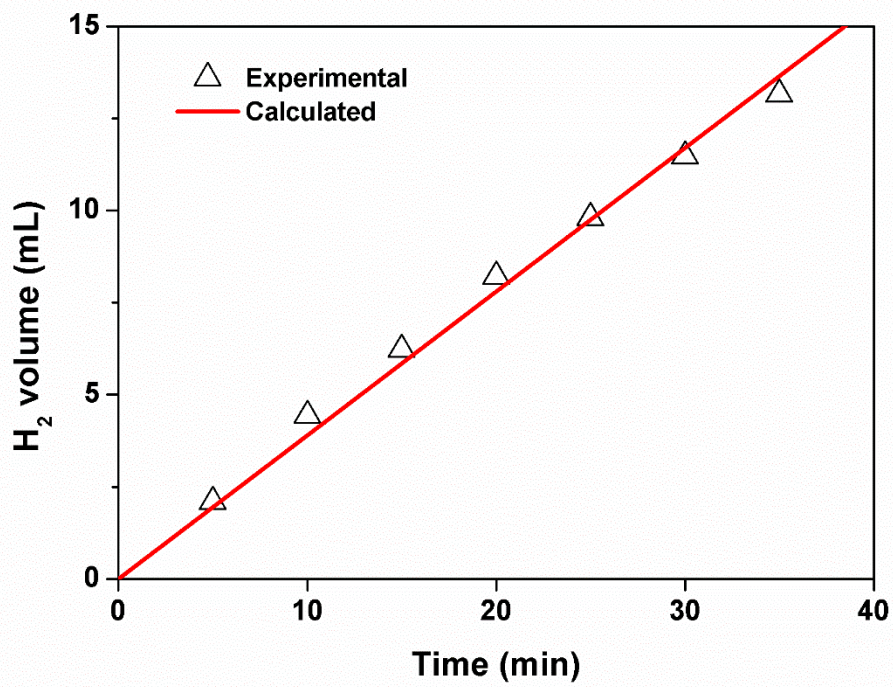


Fig. S17. The amount of H_2 theoretically calculated and experimentally measured versus time of HER on P-Mo₂C@C-2.9 with a current of 60 mA.

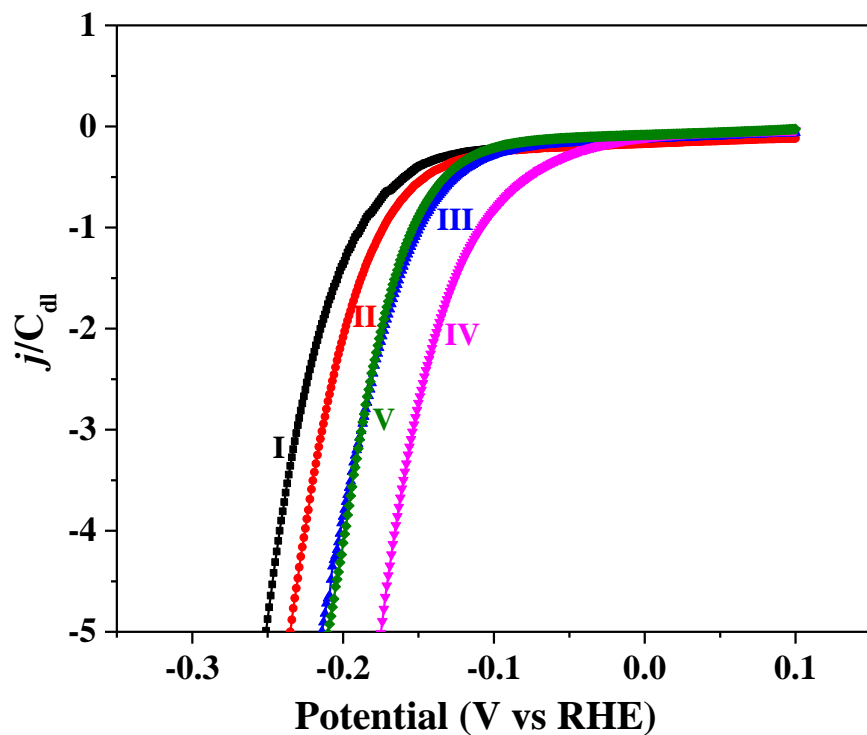


Fig. S18. Polarization curves normalized by C_{dl} of (I) $\text{Mo}_2\text{C}@\text{C}$, (II) $\text{P}-\text{Mo}_2\text{C}@\text{C}-0.8$, (III) $\text{P}-\text{Mo}_2\text{C}@\text{C}-1.9$, (IV) $\text{P}-\text{Mo}_2\text{C}@\text{C}-2.9$, and (V) $\text{P}-\text{Mo}_2\text{C}@\text{C}-3.4$.

Table S1. Summary of the texture features of P-Mo₂C@C NWs.

Catalyst	PA/An ^a	P Content (wt. %) ^b	N Content (wt. %) ^c	Mo ₂ C Content (wt. %) ^b	Free Carbon content (wt. %) ^d	Surface Mo ²⁺ percentage (%) ^e	S _{BET} (m ² g ⁻¹)
Mo ₂ C@C	0	0	0.7	35	64	36.0	41
P-							
Mo ₂ C@C-	0.01	0.8	0.8	33	65	34.8	43
	0.8						
P-							
Mo ₂ C@C-	0.025	1.9	0.7	38	59	35.4	38
	1.9						
P-							
Mo ₂ C@C-	0.05	2.9	0.7	36	60	36.9	36
	2.9						
P-							
Mo ₂ C@C-	0.1	3.4	0.6	35	61	34.6	32
	3.4						

^a Feeding Phytic acid / Aniline molar ratio in the synthesis of PA-PANI hybrid; ^b Data are calculated from EDX results;

^c Data are determined by CHN elemental analysis; ^d Data are calculated according to the results of b and c;

^e Data are determined by XPS analysis.

Table S2. Comparison of HER performance for P-Mo₂C@C nanowires with other noble-metal-free electrocatalysts in acid media.

Catalyst	Loading (mg·cm ⁻²)	j (mA·cm ⁻²)	η (mV)	Tafel slope (mV·dec ⁻¹)	Ref.
P-Mo ₂ C@C nanowires	1.30	10	89	42	This work
Co-Mo ₂ C NWs	0.14	10	140	39	<i>Adv. Funct. Mater.</i> , 2016, 27 , 5581.
MoC _x octahedrons	0.8	10	142	53	<i>Nat. Commun.</i> , 2015, 6 , 6512.
Mo ₂ C@NPC/NPRGO	0.14	10	~34 ^{&}	34	<i>Nat. Commun.</i> , 2016, 7 , 11204.
Nano-MoC@graphite shell	1.04	10	124	43	<i>J. Mater. Chem. A</i> , 2016, 4 , 6006.
MoC-RGO	0.8	—	150	57	<i>Chem. Commun.</i> , 2015, 51 , 8323.
Mo ₂ C-RGO	—	10	221	88	
Mo ₂ CNTs	0.75	10	172 ^{&}	62	<i>Angew. Chem. Int. Ed.</i> , 2015, 54 , 15395.
MoC-Mo ₂ CHNWs	0.14	10	126	43	<i>Chem. Sci.</i> , 2016, 7 , 3399.
Mo ₂ C@C	~0.28	10	124	60	<i>Angew. Chem. Int. Ed.</i> , 2015, 54 , 10752.
Mo ₂ C/CNT	2.0	10	152	65	<i>Energy Environ. Sci.</i> , 2013, 6 , 943.
np-Mo ₂ C NWs	0.21	10	~130 ^{*,&}	53	<i>Energy Environ. Sci.</i> , 2014, 7 , 387.
MoCN	0.4	10	140 ^{&}	46	<i>J. Am. Chem. Soc.</i> , 2014, 137 , 110.
N, P-Mo ₂ C@C	0.9	10	141	56	<i>ACS nano</i> , 2016, 10 , 8851.
Ni-Mo ₂ C@C	1.1	10	75 ^{&}	45	<i>J. Am. Chem. Soc.</i> , 2015, 137 , 15753.
Mo ₂ C/CNT-GR	0.65-0.67	10	130 ^{&}	58	<i>ACS nano</i> , 2014, 8 , 5164.
Mo ₂ C/RGO	0.285	10	130	57.3	<i>Chem. Commun.</i> , 2014, 50 , 13135.
MCNs@carbon	0.25	10	78 ^{&}	41	<i>Angew. Chem. Int. Ed.</i> , 2015, 54 , 14723.
W-Mo ₂ C NWs	1.28	10	~135	52	<i>Adv. Funct. Mater.</i> , 2015, 25 , 1520.
Mo ₂ C/GCSs	0.36	10	200 ^{&}	62.6	<i>ACS Catal.</i> , 2014, 4 , 2658.
Mo ₂ C-Mo ₂ N	1.4	10	177 ^{&}	—	<i>Energy Environ. Sci.</i> , 2013, 6 , 1818.
Mo ₂ C-Mo ₂ N-RGO	0.47	10	109 ^{&}	—	
CoMoS ₃	0.5	10	171	57	<i>Adv. Mater.</i> , 2016, 28 , 92.
MoO ₂ @PC-RGO	0.14	10	64 ^{&}	41	<i>Angew. Chem. Int. Ed.</i> , 2015, 54 , 12928.
WO ₂ NWs	~0.35	10	58 ^{&}	46	<i>J. Am. Chem. Soc.</i> , 2015, 137 , 6983.
Double-gyroid MoS ₂	0.022	6.74	200	43-47	<i>Nat. Mater.</i> , 2012, 11 , 963.
Edge-terminated MoS ₂	0.28	10	149	49	<i>Nat. Commun.</i> , 2015, 6 , 7493.
MoS ₂ @N-doped carbon	1.0	10	165	55	<i>Angew. Chem. Int. Ed.</i> , 2015, 54 , 7395.
Hierarchical MoS ₂	1.0	10	167	70	<i>Adv. Mater.</i> , 2015, 27 , 7426.
NiMoNx/C	0.25	2	170	36	<i>Angew. Chem. Int. Ed.</i> , 2012, 51 , 6131.
MoP NPs	0.36	10	125	54	<i>Adv. Mater.</i> , 2014, 26 , 5702.

WC-CNTs	/	10	145	72	<i>ACS nano</i> , 2015, 9 , 5125.
P-WN/rGO	0.337	10	85 ^{&}	54	<i>Angew. Chem. Int. Ed.</i> , 2015, 54 , 6423.
Ni ₂ P hollow particles	1	10	116	46	<i>J. Am. Chem. Soc.</i> , 2013, 135 , 9267.
CoP/CNT	0.285	10	122	54	<i>Angew. Chem. Int. Ed.</i> , 2014, 126 , 6828.
Cu ₃ P NWs/CF	15.2	10	143	67	<i>Angew. Chem. Int. Ed.</i> , 2014, 53 , 9577.
CoP@CC	/	10	67	51	<i>J. Am. Chem. Soc.</i> , 2014, 136 , 7587.
O-doping MoP@RGO	~0.28	10	~90 [*]	~58	<i>J. Am. Chem. Soc.</i> , 2016, 138 , 14686.

* read from the LSV curves in literatures;

[&] the HER performance with Pt foil or wire as the counter electrode;